Structural phase transitions in IrO_2 at high pressures

2008 J. Phys.: Condens. Matter 20 045202

(http://iopscience.iop.org/0953-8984/20/4/045202)

J. Phys.: Condens. Matter **20** (2008) 045202 (5pp) doi:10.1088/0953-8984/20/04/045202

Structural phase transitions in IrO_2 at high pressures

S Ono[1,2,3], J P Brodholt[1] and G D Price[1]

[1] Department of Earth Sciences, University College London, Gower Street, London WC1E 6BT, UK
[2] Institute for Research on Earth Evolution, Japan Agency for Marine-Earth Science and Technology, 2-15 Natsushima-cho, Yokosuka-shi, Kanagawa 237-0061, Japan

E-mail: shigeaki.ono@ucl.ac.uk

Received 1 August 2007, in final form 18 October 2007
Published 8 January 2008
Online at stacks.iop.org/JPhysCM/20/045202

Abstract

Structural transformations in iridium dioxide (IrO_2) were investigated using first-principles calculations up to a pressure of 50 GPa at 0 K. The phase transformation from the rutile-type to the pyrite-type structure was confirmed at 8–15 GPa. Although structures of the $CaCl_2$-type and α-PbO_2-type are observed in other metal dioxides, such as SiO_2, GeO_2, and SnO_2, our calculations indicated that these structures are metastable in IrO_2. Our calculations explain experimental observations which show the direct transformation from the rutile-type to the pyrite-type structures in IrO_2. The bulk modulus of the pyrite-type phase calculated in this study is in good agreement with the experimental value. The non-magnetic state is stable relative to the ferromagnetic and antiferromagnetic states in all IrO_2 phases. The calculated electronic density of states suggests that the pyrite-type phase is metallic.

1. Introduction

The transition metal dioxides are of great interest from a commercial point of view. For instance, iridium dioxide (IrO_2) has been used as an oxide electrode material for the production of components in advanced memory technologies [1, 2]. Under ambient conditions, IrO_2 has a rutile-type structure, which is the same as the high-pressure silica polymorph, stishovite. Among the dioxides (such as GeO_2, SnO_2 and PbO_2), IrO_2 is thought to the closest analog to silica, and thus the study of phase transitions in rutile-type IrO_2 may have geophysical implications, while also furthering our understanding of the high-pressure behavior of metal dioxides in general [3].

Recently, a new high-pressure phase of IrO_2, which has the pyrite-type structure, was synthesized at 15 GPa and ~1000 K in high-pressure experiments [4]. The pyrite-type structure was stable up to a pressure of 50 GPa. After decompression to ambient pressure and temperature, the diffraction peaks from the pyrite-type structure disappeared. This indicates that this phase is not stable under ambient conditions. A direct phase transition from the rutile-type to pyrite-type structures in IrO_2 would be interesting since other dioxides, such as silica, transform first to $CaCl_2$-type and then to α-PbO_2-type structures, before transforming at higher pressures to the pyrite-type structure [5–14]. However, the experiments of Ono *et al* [4] did not investigate pressures between 0 and 15 GPa, so they may have missed the stability fields of the $CaCl_2$-type and α-PbO_2-type structures.

Some metal dioxides with the pyrite-type structure have very high bulk moduli. For instance, SiO_2 [12], GeO_2 [15], SnO_2 [13], and RuO_2 [16] all have bulk moduli higher than 300 GPa. The pyrite-type IrO_2 also has a high bulk modulus (~300 GPa) [4]. A high bulk modulus is one of the indicators of ultra-hard materials and, since ultra-hard materials are currently of interest from an industrial aspect, it is also worthwhile investigating the physical properties of pyrite-type IrO_2.

In this study, we used density functional theory to investigate the enthalpies of possible IrO_2 phases as predicted by the transition sequences of analog dioxide materials. We also investigate the physical properties of IrO_2 phases, and discuss the absences of the $CaCl_2$-type and the α-PbO_2-type phases in high-pressure experimental studies [4].

2. Computational procedure

Ab initio calculations carried out in this study were based on density functional theory using the VASP package [17].

[3] Address for correspondence: Department of Earth Sciences, University College London, Gower Street, London WC1E 6BT, UK.

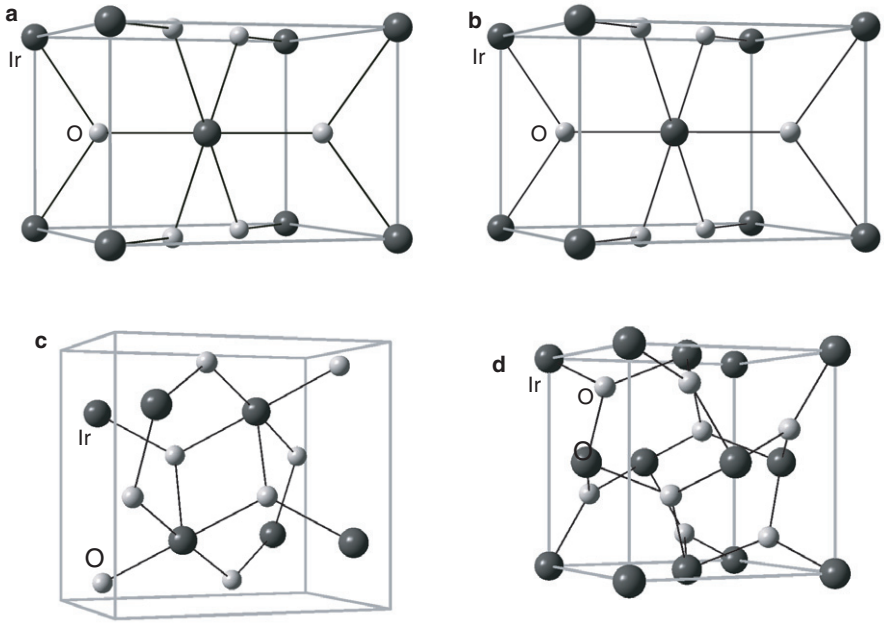

Figure 1. Structures of IrO_2 phases. Dark and light gray squares denote Ir and O atoms, respectively. Light gray boxes denote the outline of the unit cells: (a) rutile-type; (b) $CaCl_2$-type; (c) α-PbO_2-type; (d) pyrite-type. The difference between the rutile- and the $CaCl_2$-type phases is due to the splitting of cell parameter from a to a and b, induced by the change in the atomic positions of oxygen.

We used the local density approximation (LDA) [18] and the generalized gradient approximation (GGA) [19] for the exchange–correlation functional. The electronic wave functions are expanded in a plane-wave basis set with a cutoff energy of 700 eV, and the electron–ion interaction is described by means of the projector augmented wave (PAW) method [20, 21]. The core radii are 2.60 au for Ir and 1.52 au for O, respectively. Integration over the Brillouin zone was performed using a Monkhorst–Pack grid, with the number of irreducible k-points ranging from 76 to 216 depending on the cell size and symmetry. The equilibrium structure was obtained after full geometry optimization using the conjugate gradients method. The total energies converged to within 1 meV per atom. We calculated the ferromagnetic and the antiferromagnetic spin configurations to assess the stabilities of the spin states. The calculated results for all phases showed that the non-magnetic state is most stable. Therefore, we investigated only non-magnetic phases in the rest of this study. Elastic constants of the rutile-type phase were obtained from evaluations of the stress tensor generated by small strains. We performed the spin–orbit coupling calculation to assess the influence of the relativistic effect. The volume difference of the rutile-type IrO_2 between calculations with and without spin–orbit coupling was 0.7% at ambient pressure. This volume difference was much smaller than that between different exchange–correlation functionals (LDA and GGA). Therefore, the spin–orbit coupling effect was not considered in this study. A comprehensive review of our methodology has been given elsewhere [22]. The bulk moduli of each phase were evaluated by fitting the results to a Birch–Murnaghan equation of state.

3. Results and discussion

Four structures, rutile-, $CaCl_2$-, α-PbO_2- and pyrite-type, were calculated in this study (figure 1). The rutile-type phase is stable under ambient conditions, while the pyrite-type phase has been observed at high pressure. On the other hand, there is no experimental report of an appearance of the $CaCl_2$- or α-PbO_2-type phases. However, both structures have been observed in not only metal dioxides but also other AX_2 compounds, such as fluorides and hydrides [23–25]. The optimized structures of all phases at 0 GPa in this study are shown in table 1. The differences in cell parameters and atomic coordinates between the rutile- and the $CaCl_2$-type phases are very small, as expected in a second-order ferroelastic phase transition. The coordination number of Ir^{4+} cations in all structures, except for the pyrite-type structure, is six. The coordination number in the pyrite-type structure shows a transition state from six to eight.

We calculated the bulk moduli of all structures at 0 K using both LDA and GGA (table 2). Volumes at 0 GPa from LDA are smaller than those from GGA. In contrast, bulk moduli from LDA are higher than those from GGA. The interesting feature is that the bulk modulus and its first pressure derivative of the α-PbO_2-type phase is much smaller those of other phases. This may indicate that the α-PbO_2-type phase is not stable at high pressures.

The enthalpy differences between the phases were calculated to confirm the pressure conditions where each phase is stable. The enthalpy was obtained directly in our calculations as $H = E + PV$, where E is the internal energy. The enthalpy of the rutile-type phase is almost the same as that of the $CaCl_2$-type phase. The difference is less than 0.1 eV

Table 1. Structures of calculated phases in IrO_2. (Note: cell parameters and atomic coordinates of all phases were calculated at 0 GPa. Full optimized calculations were performed using LDA and GGA. Values from GGA are in parentheses.)

	Rutile	$CaCl_2$	α-PbO_2	Pyrite
Space group	$P4_2/mnm$	$Pnnm$	$Pbcn$	$Pa\bar{3}$
Z	2	2	4	4
		Cell parameters		
a (Å)	4.448 (4.541)	4.451 (4.544)	4.173 (4.332)	4.843 (4.933)
b (Å)		4.446 (4.539)	5.605 (5.667)	
c (Å)	3.148 (3.191)	3.148 (3.191)	5.248 (5.307)	
V (Å^3)	62.28 (65.79)	62.30 (65.80)	122.75 (130.29)	113.58 (120.02)
		Atomic coordinates		
Ir	2a	2a	4c	4a
x	0 (0)	0 (0)	0 (0)	0 (0)
y	0 (0)	0 (0)	0.1418 (0.1422)	0 (0)
z	0 (0)	0 (0)	0.25 (0.25)	0 (0)
O	4f	4g	8d	8c
x	0.3091 (0.3085)	0.3094 (0.3088)	0.2606 (0.2620)	0.3499 (0.3491)
y	0.3091 (0.3085)	0.3087 (0.3081)	0.3867 (0.3869)	0.3499 (0.3491)
z	0 (0)	0 (0)	0.4209 (0.4200)	0.3499 (0.3491)

Table 2. Bulk moduli and volumes of IrO_2 phases at 0 K. (Note: the Birch–Murnaghan equation of state was used to calculate the bulk moduli of IrO_2 phases—B_0 is the isothermal bulk modulus, B_0' the first pressure deviation of the bulk modulus, V_0 the volume at 0 GPa.)

		B_0 (GPa)	B_0'	V_0 (Å^3)
LDA				
	Rutile	314.5	4.48	62.28
	$CaCl_2$	315.9	4.44	62.30
	α-PbO_2	258.7	2.62	122.73
	Pyrite	352.7	4.51	113.56
GGA				
	Rutile	266.0	4.57	65.78
	$CaCl_2$	269.4	4.47	65.77
	α-PbO_2	231.0	2.82	130.29
	Pyrite	297.1	4.61	120.02
Experiment[a]				
	Pyrite	306	4 (fixed)	115.9

[a] Experimental values were reported in Ono *et al* [4].

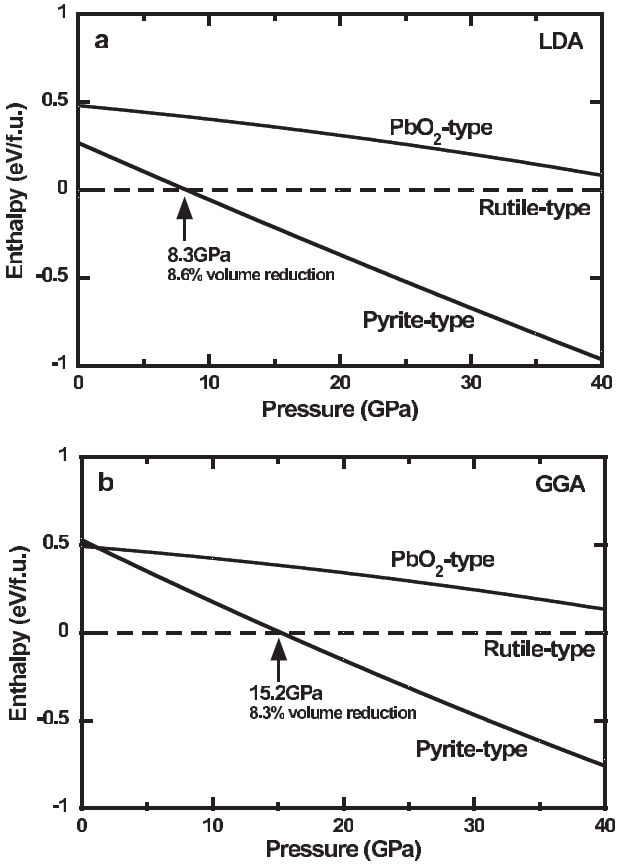

Figure 2. Transition pressures of IrO_2 at 0 K. The solid lines denote the enthalpy differences of the α-PbO_2-type and pyrite-type phases relative to the rutile-type phase as a function of pressure: (a) LDA; and (b) GGA. The transition pressures from the rutile structure to the pyrite structure are 8.3 and 15.2 GPa from the GGA and LDA calculations, respectively.

at the pressures investigated in this study. Therefore, it is difficult to assess the stability of the $CaCl_2$-type phases using the enthalpies. Figure 2 shows the enthalpy differences of the α-PbO_2- and the pyrite-type phases with respect to the rutile-type phase. The results show that a phase transition from the rutile- to the pyrite-type structures occurs at 8.3 and 15.2 GPa from LDA and GGA, respectively. This phase transition results in a volume reduction of ∼8.5%. In contrast, there is no stability field for the α-PbO_2-type phase. This result is consistent with the speculation made from the predicted low bulk modulus of the α-PbO_2-type phase.

Due to the small enthalpy difference between the rutile- and $CaCl_2$-type phases, we have used an alternative analysis to assess their relative stability. It is known that rutile-type to $CaCl_2$-type transitions involve softening of the $C_{11} - C_{12}$ shear modulus and Raman B_{1g} mode with increasing pressure [5, 9, 26]. Therefore, the transition pressure can be predicted using the change in elastic constants. We derive elastic constants from the *ab initio* results by calculating the second derivatives of the energy density (which is defined as total energy (E) per volume) as a function of appropriately

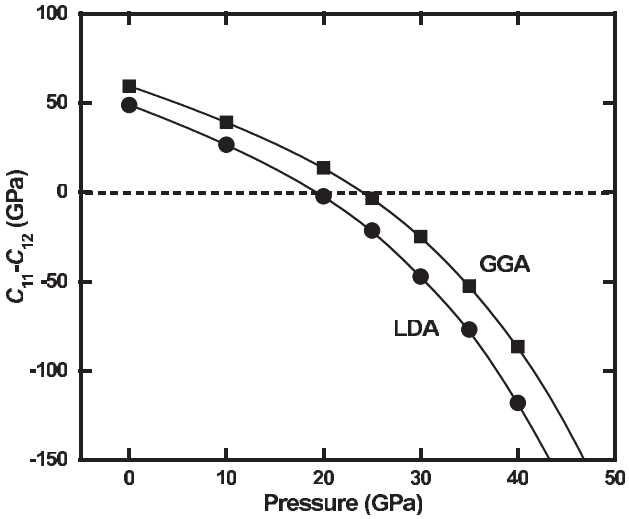

Figure 3. Pressure dependence of the shear $C_{11} - C_{12}$ of the rutile-type IrO_2. The solid circles and squares denote the values calculated by LDA and GGA. The strain parameter (x) was set to 0.03. The intersection at 0 GPa in $C_{11} - C_{12}$ indicates the phase transition from the rutile- to the $CaCl_2$-type structure. The transition pressures were 20 and 25 GPa from LDA and GGA calculations, respectively.

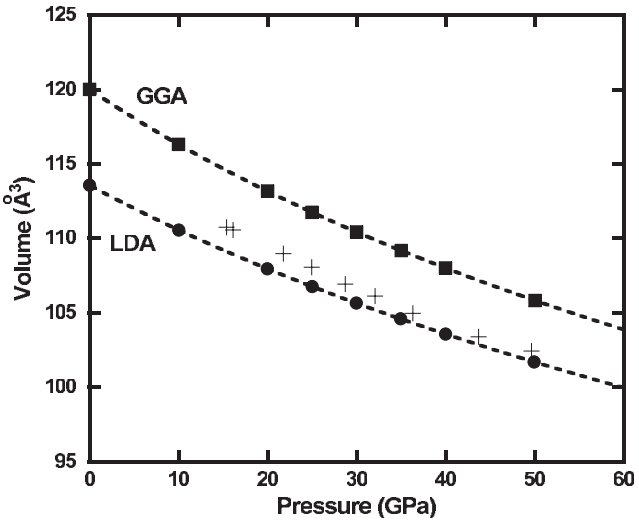

Figure 4. The volume of the pyrite-type IrO_2 as a function of pressure at 0 K. The solid circles and squares denote volumes calculated by LDA and GGA, respectively. Crosses are experimental values at 300 K, reported in Ono *et al* [4].

chosen lattice distortions (e_i) [27]. A tetragonal crystal structure has six independent elastic constants. We have constructed the strain (ε) to get $C_{11} - C_{12}$ in the following way:

$$\varepsilon = \begin{pmatrix} e_1 & 0 & 0 \\ 0 & e_2 & 0 \\ 0 & 0 & 0 \end{pmatrix}, \qquad \text{where } e_1 = \left[\frac{(1+x)}{(1-x)}\right]^{\frac{1}{2}} - 1$$

$$\text{and} \qquad e_2 = -\frac{e_1}{(1+e_1)}. \tag{1}$$

Then, the relationship of the elastic constant is calculated from the change in the total energy per volume by

$$\frac{\Delta E}{V} = (C_{11} - C_{12})\, x^2, \tag{2}$$

where x is the strain parameter. The ions were allowed to fully relax in the deformed cell.

Figure 3 shows the change in the shear modulus of $C_{11} - C_{12}$ as a function of pressure. $C_{11} - C_{12}$ decreases with pressure, and we find that $C_{11} - C_{12} = 0$ at 20 and 25 GPa from LDA and GGA calculations, respectively. This indicates that the transition pressure from the rutile- to the $CaCl_2$-type phases is 20–25 GPa. At these pressures, however, as shown in figure 2, the enthalpy of the pyrite-type phase is significantly lower than both these phases. We conclude, therefore, that the $CaCl_2$-type structure in IrO_2 is not stable at high pressures.

The volume of the pyrite-type phase as a function of pressure is shown in figure 4. The calculated volumes from LDA are smaller than those from GGA. The experimental data are also plotted [4], indicating that the observed volumes are between the LDA and GGA predictions. As it is known that the LDA and GGA calculations generally underestimate and overestimate volumes respectively, our calculations are in general agreement with the experimental observations. The calculated volumes using LDA are closer to the experimental values as pressure increases. In contrast, the bulk modulus calculated using GGA agrees with the experimental result (table 2).

Table 3. Elastic constants of pyrite-type IrO_2. (Note: all values are in GPa.)

		C_{11}	C_{12}	C_{44}
LDA				
	0 GPa	564	299	178
	20 GPa	649	386	194
GGA				
	0 GPa	454	213	155
	20 GPa	572	319	176

The elastic stiffness tensor relates to the stress tensor and the strain tensor according to Hooke's law. As the stress and strain tensors are symmetric, the most general elastic stiffness tensor has 21 non-zero independent components. In the case of the cubic crystal, the elastic stiffness coefficients (elastic constants) are reduced to three components: C_{11}, C_{12}, and C_{44} (in the Voigt notation). Elastic constants of the pyrite-type phase at 0 and 20 GPa are shown in table 3. Both C_{11} and C_{12} increase with increasing pressure, whereas the slope for C_{44} is relatively low. All the values of elastic constants calculated by LDA are higher than those calculated by GGA.

In figure 5, we show the electronic density of states (EDOS) for the rutile-type and the pyrite-type phases. In the case of the rutile-type phase (figure 5(a)), the lower energy band formed by oxygen 2s electrons is ∼20 eV below the Fermi energy. The upper energy band is formed by hybridization between oxygen 2p and iridium 5d electrons. At the Fermi energy level, there is no band gap in the total EDOS, indicating that this phase should be metallic. The conduction band is mostly iridium 5d electrons. These results are in good agreement with previous studies [28–30]. For the pyrite-type phase (figure 5(b)) there is also no band gap at the Fermi energy

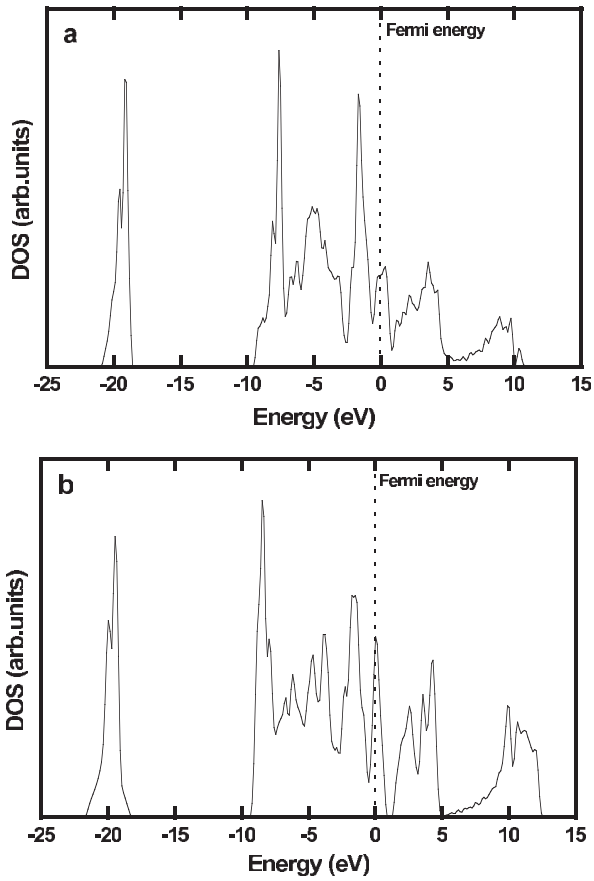

Figure 5. Total density of states of IrO_2 phases at 0 K. The Fermi level is set as the zero of energy and is indicated by the dashed lines: (a) the rutile-type structure at 0 GPa; and (b) the pyrite-type structure at 20 GPa.

level in the total EDOS, indicating that this phase should also be metallic. The peak position of the lower band formed by oxygen 2s electrons is 0.3 eV lower than that of the rutile-type phase. The conduction band is composed mainly of Ir 5d electrons, which are split into ∼3 and ∼8 eV. The EDOS near the Fermi energy level is dominated by the contribution from oxygen 2p and iridium 5d electrons.

4. Concluding remarks

Our calculations have shown a direct phase transition from the rutile-type to the pyrite-type phase at 8–15 GPa without any appearances of the $CaCl_2$-type and α-PbO_2-type phases. This result explains why these two phases had not be observed in previous experiments. In the case of other metal dioxides, such as SiO_2, GeO_2, and SnO_2, the two structures of the $CaCl_2$-type and α-PbO_2-type are observed at high pressures [5, 7, 9–11, 13, 14, 26]. In contrast, RuO_2 shows an absence of the α-PbO_2-type phase [16]. As the ionic radius of Ru^{4+} is almost equal to that of Ir^{4+} and both elements belong to the platinum group metals, these metal dioxides are likely to prefer the absence of the α-PbO_2-type phase. The pyrite-type structure is commonly observed at high pressure in many metal dioxides, which have the rutile-type structure at ambient and low pressures. The bulk moduli of the pyrite-type structure of most metal dioxides are higher than 300 GPa. This indicates that some of pyrite-type phases could be potential candidates for advanced ultra-hard materials with industrial significance, if the pyrite-type phase can be acquired under ambient conditions.

Acknowledgments

The authors thank S Taioli and A S Côté for their valuable help. This work made use of the University College London (UCL) research computing facilities and of HPCx, the UK's national high-performance computing service at the Daresbury Laboratory. This work was supported by Natural Environment Research Council (NERC) Computational Mineral Physics Consortium, UK and a Grant-in-Aid for Scientific Research from the Ministry of Education, Culture, Sport, Science and Technology, Japan.

References

[1] Hackwood S, Beni G, Bösch M A, Kang K, Schiavone L M and Shay J L 1982 *Phys. Rev.* B **26** 7073
[2] Igarashi Y, Tani K, Kasai M, Ahikaga K and Ito T 2000 *Japan. J. Appl. Phys.* **39** 2083
[3] Haines L, Léger J M and Schutle O 1996 *Science* **271** 629
[4] Ono S, Kikegawa T and Ohishi Y 2005 *Physica* B **363** 140
[5] Kingma K J, Cohen R E, Hemley R J and Mao H K 1995 *Nature* **374** 243
[6] Haines L, Léger J M and Schutle O 1996 *J. Phys.: Condens. Matter* **8** 1631
[7] Haines L and Léger J M 1997 *Phys. Rev.* B **55** 11144
[8] Teter D M and Hemley R J 1998 *Phys. Rev. Lett.* **80** 2145
[9] Haines J, Léger J M, Chateau C, Bini C R and Ulivi L 1998 *Phys. Rev.* B **58** R2909
[10] Ono S, Hirose K, Murakami M and Isshiki M 2002 *Earth Planet. Sci. Lett.* **197** 187
[11] Ono S, Tsuchiya T, Hirose K and Ohishi Y 2003 *Phys. Rev.* B **68** 134108
[12] Oganov A R, Gillan M J and Price G D 2005 *Phys. Rev.* B **71** 064104
[13] Ono S, Funakoshi K, Nozawa A and Kikegawa T 2005 *J. Appl. Phys.* **97** 073523
[14] Shieh S R, Duffy T S and Shen G 2005 *Earth Planet. Sci. Lett.* **235** 273
[15] Jolly L H, Sivi B and d'Arco P 1994 *Eur. J. Mineral.* **6** 7
[16] Haines J and Léger J M 1993 *Phys. Rev.* B **48** 13344
[17] Kresse G and Furthmüller J 1996 *Phys. Rev.* B **54** 11169
[18] Kohn W and Sham L J 1965 *Phys. Rev.* A **140** 1133
[19] Wang Y and Perdew J P 1991 *Phys. Rev.* B **44** 13298
[20] Blöchl P E 1994 *Phys. Rev.* B **50** 17953
[21] Kresse G and Joubert D 1999 *Phys. Rev.* B **59** 1758
[22] Gillan M J, Alfè D, Brodholt J P, Vočadlo L and Price G D 2006 *Rep. Prog. Phys.* **69** 2365
[23] Perakis A, Lampakis D, Boulmetis Y C and Raptis C 2005 *Phys. Rev.* B **72** 144108
[24] Yubuta K, Hongo T, Atou T, Nakamura K G, Kondo K and Kikuchi M 2007 *Solid State Commun.* **143** 127
[25] Vajeeston P, Ravindran P, Hauback B C, Fjellvag H, Kjekshus A, Furuseth S and Hanfland M 2006 *Phys. Rev.* B **73** 224102
[26] Hellwig H, Goncharov A F, Gregoryanz E, Mao H K and Hemley R J 2003 *Phys. Rev.* B **67** 174110
[27] Mehl M J, Osburn J E, Paraconstantopoulos D A and Klein B M 1990 *Phys. Rev.* B **41** 10311
[28] Goel A K, Skorinko G and Pollak F H 1981 *Phys. Rev.* B **24** 7342
[29] Xu J H, Jarlborg T and Freeman A J 1989 *Phys. Rev.* B **40** 7939
[30] de Almeida J S and Ahuja R 2006 *Phys. Rev.* B **73** 165102